Smart Structures and Systems, *Vol. 23, No. 5 (2019) 479-493*
DOI: https://doi.org/10.12989/sss.2019.23.5.479

Experimental and numerical studies of the pre-existing cracks and pores interaction in concrete specimens under compression

Hadi Haeri[1], Vahab Sarfarazi[2], Zheming Zhu[*1] and Mohammad Fatehi Marji[3]

[1]*MOE Key Laboratory of Deep Underground Science and Engineering, School of Architecture and Environment,Sichuan University, Chengdu 610065, China*
[2]*Department of Mining Engineering, Hamedan University of Technology, Hamedan, Iran*
[3]*Department of Mining Engineering, Yazd University, Yazd, Iran*

(Received January 30, 2019, Revised March 16, 2019, Accepted March 19, 2019)

Abstract. In this paper, the interaction between notch and micro pore under uniaxial compression has been performed experimentally and numerically. Firstly calibration of PFC2D was performed using Brazilian tensile strength, uniaxial tensile strength and biaxial tensile strength. Secondly uniaxial compression test consisting internal notch and micro pore was performed experimentally and numerically. 9 models consisting notch and micro pore were built, experimentally and numerically. Dimension of these models are 10 cm *10 cm* 5 cm. the length of joint is 2 cm. the angularities of joint are 30°, 45° and 60°. For each joint angularity, micro pore was situated 2cm above the lower tip of the joint, 2 cm above the middle of the joint and 2 cm above the upper of the joint, separately. Dimension of numerical models are 5.4 cm*10.8 cm. The size of the cracks was 2 cm and its orientation was 30°, 45° and 60°. Diameter of pore was 1cm which situated at the upper of the notch i.e., 2 cm above the upper notch tip, 2 cm above the middle of the notch and 2 cm above the lower of the notch tip. The results show that failure pattern was affected by notch orientation and pore position while uniaxial compressive strength is affected by failure pattern.

Keywords: experimental tests; notch and micro pore interaction; bonded particle method; discrete element method

1. Introduction

Concretes used in the construction of engineering structures may contain several natural weaknesses in form of pores, micro cracks, grains boundaries and the laminations between the layers known as bedding planes. These pre-existing defects may eventually induce macro cracks due to internal or external forces endeavored by the concrete structures (Wang and Kemeny 1994, Marji 2014, Haeri 2015a). On the other hand, presence of these natural defects near the crack tips may change the stress and displacement fields near these singular points and may lead to changing the elastic behavior of the material near the tips to that of plastic. These processes can produce the plastic zones of different sizes and shapes depending the materials being used and the loading conditions being endeavored by the concrete structures. The fracturing characteristics of the concretes may be defined in form of fracture toughness and the crack extension and crack kinking phenomena. Therefore, the shape and size of crack tip plastic zones and the crack growing process in form of crack length, initiation of crack propagation, crack growth length, crack initiation and propagation angles and crack growth rate considering the presence of other defects such as pores and planes of weaknesses may all be studied to have a good understanding of concrete behavior and concrete failure process which is very helpful in the engineering design of different concrete structures under different loading conditions (Haeri *et al.* 2015a, b, Marji 2014). The linear elastic fracture mechanics concepts can be effectively used for the crack analyses of brittle materials such as concretes and rocks. The linear elastics stress analysis near the crack tips can be used to predict the stress and displacement fields near these singular points where the inelastic deformation can be produced in both ductile and brittle materials (Marji 2014, 2015, Abdollahipour *et al.* 2015). Plastic deformation in form of plastic strains may develop in most concrete materials near the crack tips when the yield strength of the material is exceeded. The concretes remain elastic during the loading procedure before the yield strength of the specimen. However, the formation of plastic zone in concrete depends on the material properties, loading conditions and structural element configuration. The moderate crack tip yielding can be used to estimate the size of plastic zone for a particular concrete specimen e.g. the Von-Mises yield criterion and the associated flow rules as used by some researchers (Rice and Rosengren 1968, Kuang and Chen 1997). A vast number of analytical, experimental and numerical studies has been carried out to study the elastic interaction between a crack and micro defects in homogeneous solid materials (Rose 1986, Rubinstein 1986, Horii and Nemat-Nasser 1987, Yang 2011, Yoshihara 2013, Zeng *et al.* 2014, Jiang *et al.* 2014, Haeri 2015b, Haeri *et al.* 2016a,b, and Haeri, 2016). Manystudies have been carried out to determine the plastic behaviour near the crack tip (Bian 2004, Botvina 2005, Tong 2007, Antunes 2008, ASTM 2008, Oudad 2009,

*Corresponding author, Professor
E-mail: zhemingzhu@hotmail.com

ISSN: 1738-1584 (Print), 1738-1991 (Online)

Kudari 2009, Rans 2009, Kudari 2009, Gao 2010, Huang 2010, Gao 2010, Xin 2010, Caputo 2012, Castro 2013, Sousa 2013, Nabil *et al*. 2012, Ramadoss 2013, Caputo 2013, Pan 2014, Nejati and Ghazvinian 2014, Panaghi *et al*. 2015, Nabil *et al.* 2017, Monfared 2017, Boumaaza *et al*. 2017, Rooh *et al.* 2018, Khodayar and Nejati 2018). Several researchers have been done the experimental study on the pre-existing cracks and pores interaction (Cheng *et al*. 2016, Zhou *et al.* 2018a,b, Zhang *et al.* 2018).

Many numerical methods can be applied to investigate interaction between internal notch and micro pore, such as General Particle Dynamics (GPD) (BI *et al.* 2016, Bi *et al.* 2017, Zhou 2018a). Peridynamics(PD) (Wang *et al.* 2016, Wang *et al*. 2017, Wang *et al.* 2018), The Extended Finite Element Method (Cheng 2015).

However, the plastic deformation around the crack tips in isotropic materials occurs identically in all directions and can be mathematically formulated based on the classical theory of plasticity because in this case, there is no preferred direction for the plastic deformation. When the crack tip is near a micro-defect, the situation significantly differs because these defects influence on the size and shape of the crack tips plastic zone. Therefore, in this study, the effects of interaction of micro pore and internal joints (near the tip of the crack) are investigated for a typical concrete specimen (containing micro pores and pre-existing cracks) under compression. The aim of this research is to investigate the crack propagation and crack growth processes by experimental tests carried out on the specially prepared laboratory concrete specimens and also by discrete element simulation of the modeled concrete samples using the bonded particle model (BPM) implemented in particle flow code in two dimension (PFC2D).

2. Laboratory tests and results

Several laboratory tests have been carried out to study the effects of the crack and micro pore interaction on the crack propagation and failure processes of concrete specimens under compression. Some experimental tests were also conducted to calibrate the numerical models developed for the numerical investigation of the pore-crack interaction effects on the fracture process of modeled concrete specimens.

2.1 Preparing the modeled samples

A mixture of plaster, cement, and water is used for producing the intact specimens and the specimens with pre-existing pore-cracks. The mixture is made of equal proportions of cement, plaster, and water by weight. A mixer was used for missing the batches for exactly 10 minutes. The flow able mixture was then cast in the molds and cured at the room condition with the temperature of at 20±2°C in the geo-mechanics laboratory for 20 days. The cylindrical molds were 54 mm in diameter and 108 mm in height (height to diameter ratio of 2) and the disc specimens were 54 mm in diameter and 27 mm in thickness.

Table 1 Experimentally determined properties of intact modeled samples

Mechanical properties	Experimental results
Elastic modulus (GPa)	17
Poisson's ratio	0.18
UCS (MPa)	10
Crack initiation stress (MPa)	7
Brazilian tensile strength (MPa)	1.3
Friction angle	29
Cohesion (MPa)	3

2.2 The mechanical properties of the intact material used for the modeled samples

To characterize the mechanical properties of the molded specimen, several different tests in uniaxial compression, biaxial compression, and Brazilian configurations were conducted. Table 1 provides a summary of the mechanical properties of the intact concrete materials obtained from the experiments.

2.3 Preparing and testing the models consisting crack and pore

In this research, the concrete specimens containing cracks and pores are specially prepared in the laboratory by using a mold with 100 mm in length and width and 50 mm in thickness. The concrete specimen was a mixture of fine sand, cement and water by a ratio of 0.4/1/1. Fiberglass sheets containing smooth contact surfaces are attached together to prepare the specially designed mold for preparing the concrete specimens in the laboratory. The fiberglass plates of 20 mm in thickness are placed on the top and bottom of the mold to produce the concrete specimens with smooth surfaces. The top plate contains two orifices allowing the cast able concrete material mortar to flow into the enclosed mold. Slits of 1 mm aperture are placed at the upper and lower surfaces of the mold. The length of these slits is equal to the thickness of the modeled specimens. One shim and one cylinder are inserted into the mold to leave the required spaces for simulating the internal crack and pore respectively after poring the gypsum. The casted specimens were kept in the mold for 7 hours then unmolded and kept in the laboratory at the temperature of 20±2°C (room temperature) for 20 days. The shim and cylinder are greased and placed with in the casted specimen to produce smooth through thickness cracks and pore. It has been tried to produce open natural crack with smooth surfaces while removing the shims from the concrete specimen. Repeating the same procedure for nine specimens, the required concrete specimens containing non-persistent crack and pore were prepared so that the size of crack was 2 cm and its orientation was changed for each specimen as: 30° (Fig. 1), 45° (Fig. 2) and 60° (Fig. 3), respectively. In addition, the pore had a diameter of 1 cm and was placed 2 cm either above the upper tip of the crack, or 2 cm bellow the lower crack tip or 2 cm above or below the center of the crack in any individual concrete specimen.

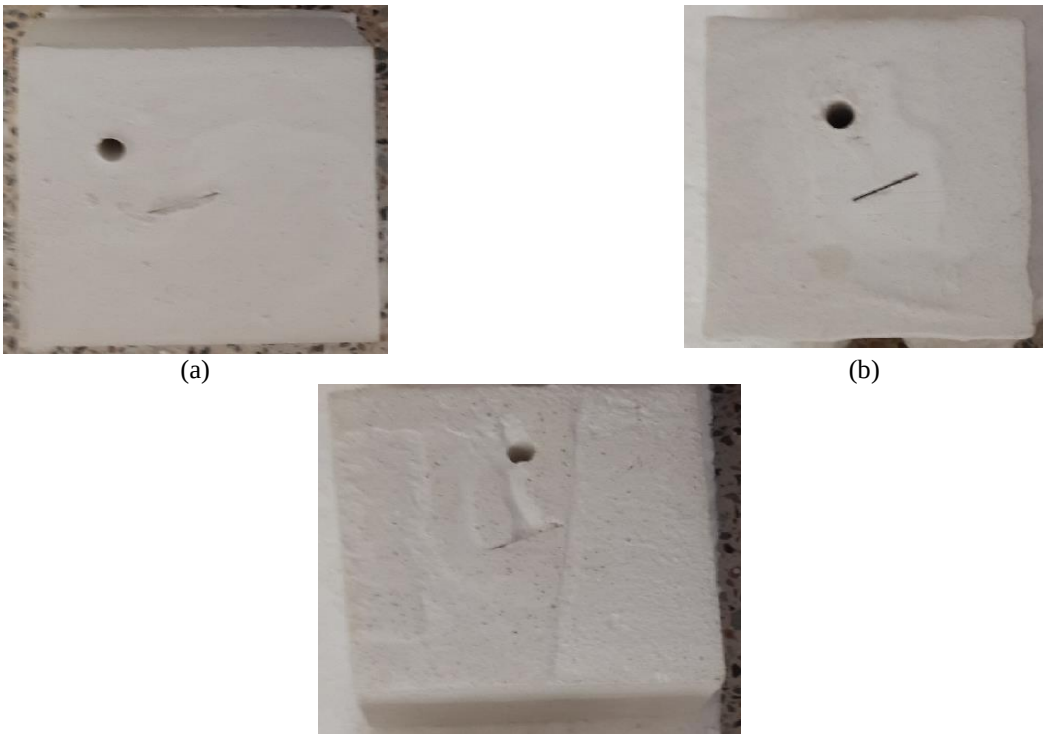

(a) (b)

(c)

Fig. 1 Pore was situated (a) 2 cm above the upper notch tip, 2 cm above the middle of the notch and 2 cm above the lower of the notch tip; notch angle is 30°

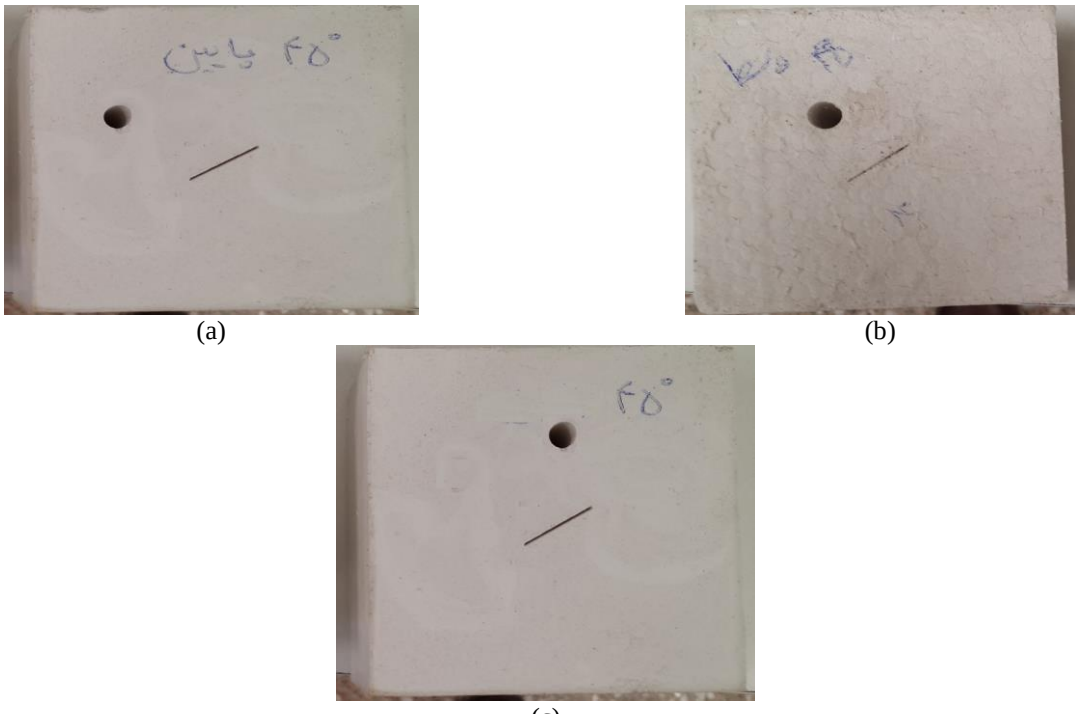

(a) (b)

(c)

Fig. 2 Pore was situated (a) 2 cm above the upper notch tip, 2 cm above the middle of the notch and 2 cm above the lower of the notch tip; notch angle is 45°

The uniaxial compression test machine was used for testing the sample. The loading rate was 0.01 mm/s. after the test, the broken samples was check visually and failure pattern and failure mode were determined.

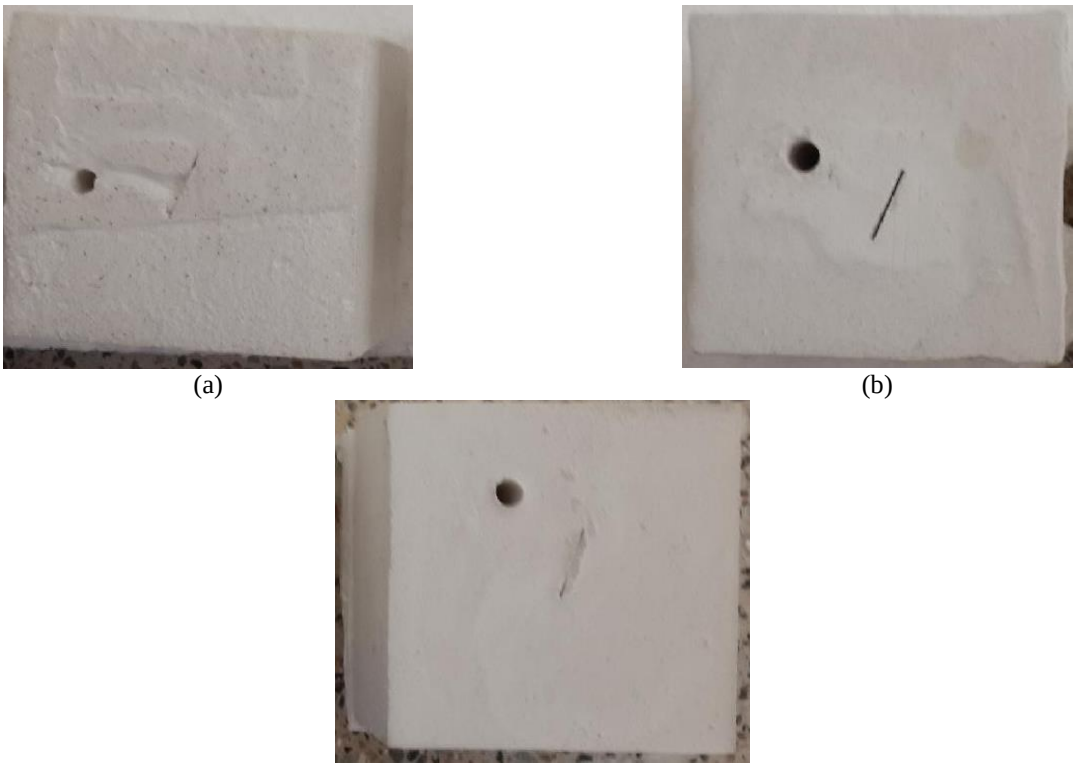

(a) (b)

(c)

Fig. 3 Pore was situated (a) 2 cm above the upper notch tip, 2 cm above the middle of the notch and 2 cm above the lower of the notch tip; notch angle is 60°

3. Fracturing patterns in loaded specimens consisting pore and crack

The fracture patterns of specimens containing different pore and notch configurations are discussed in this section. The fracturing patterns are categorized by considering different angle of notches including, 30°, 45° and 60°, and different pore's situation as shown in Figs. 1- 3 respectively.

3.1 Specimens with notch angle 30°

When notch angle is 30° and pore was situated 2 cm above the upper tip of the joint (Fig. 4(a)), two wing crack initiate from notch tips and propagate nearly parallel to normal load till coalescence with sample edge. Also three wing cracks initiate from the hole. One of these crack coalesce with lower tip of the notch and two of them coalescence with sample edge.
When notch angle is 30° and pore was situated 2 cm above the middle of the joint (Fig. 4(b)), three wing crack initiate from notch tips and propagate till coalescence with sample edge. Also three wing cracks initiate from the hole. Two of these crack coalesce with the notch and one of them coalescence with sample edge.
When notch angle is 30° and pore was situated 2 cm above the lower tip of the joint (Fig. 4(c)), two wing crack initiate from notch tips and propagate nearly parallel to normal load till coalescence with sample edge. Also two wing cracks initiate from the hole. One of these crack coalesce with the notch and one of them coalescence with sample edge.

3.2 Specimens with notch 45°

When notch angle is 45° and pore was situated 2 cm above the upper tip of the joint (Fig. 5(a)), two wing crack initiate from notch tips and propagate nearly parallel to normal load till coalescence with sample edge. Also three wing cracks initiate from the hole. One of these crack coalesce with lower tip of the notch and two of them coalescence with sample edge.
When notch angle is 45° and pore was situated 2 cm above the middle of the joint (Fig. 5(b)), one wing crack initiate from upper tip of the notch and propagate nearly parallel to normal load till coalescence with sample edge. Also two wing cracks initiate from the hole. One of these crack coalesce with lower tip of the notch and one of them coalescence with sample edge.
When notch angle is 45° and pore was situated 2 cm above the lower tip of the joint (Fig. 5(c)), two wing crack initiate from the notch and propagate nearly parallel to normal load till coalescence with sample edge. Also two wing cracks initiate from the hole. One of these crack coalesce with lower tip of the notch and one of them coalescence with sample edge.

3.3 Specimens with notch 60°

When notch angle is 60° and pore was situated 2 cm above the upper tip of the joint (Fig. 6(a)), two wing crack initiate from the notch and propagate nearly parallel to normal load till coalescence with sample edge. Also two

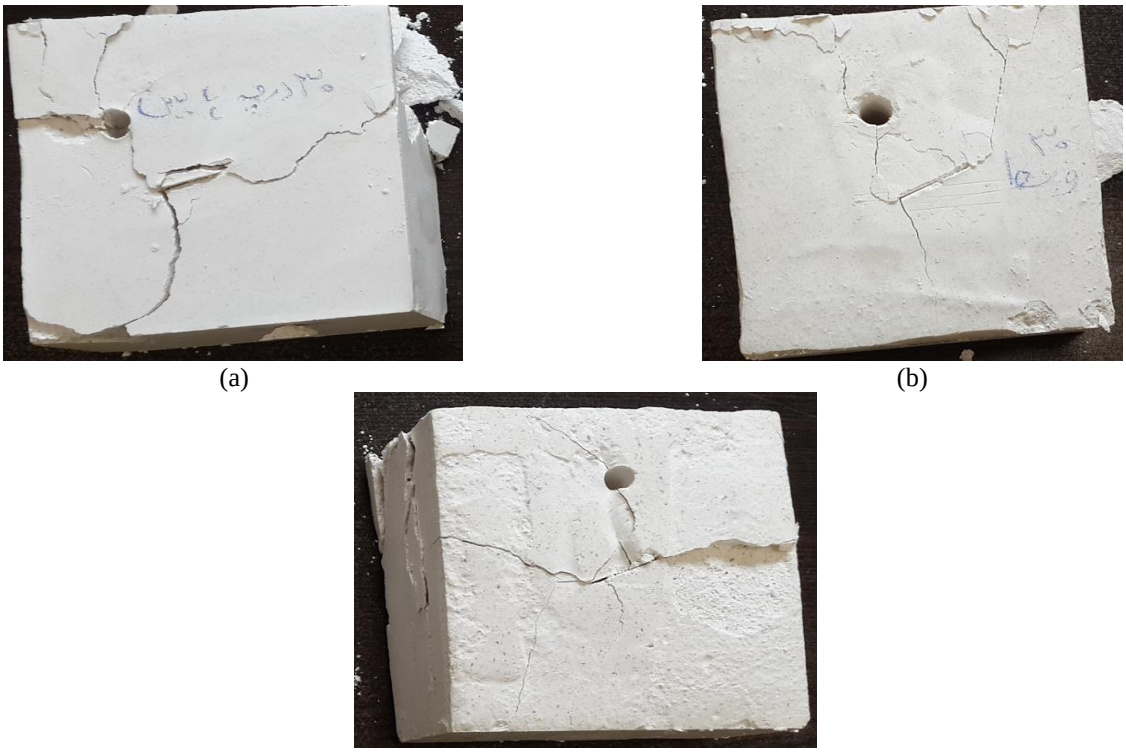

(a) (b)

(c)

Fig. 4 Failure pattern when Pore was situated (a) 2 cm above the upper notch tip, 2 cm above the middle of the notch and 2 cm above the lower of the notch tip; notch angle is 30°

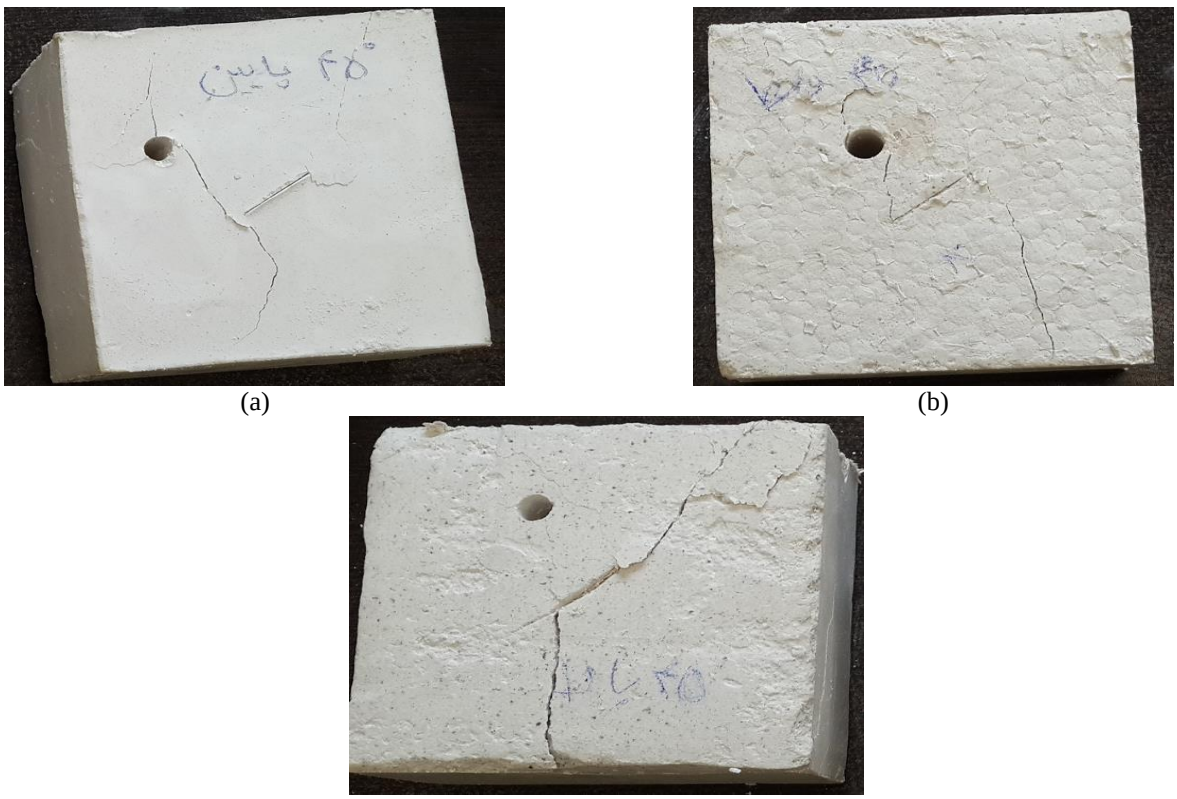

(a) (b)

(c)

Fig. 5 Failure pattern when Pore was situated (a) 2 cm above the upper notch tip, 2 cm above the middle of the notch and 2 cm above the lower of the notch tip; notch angle is 45°

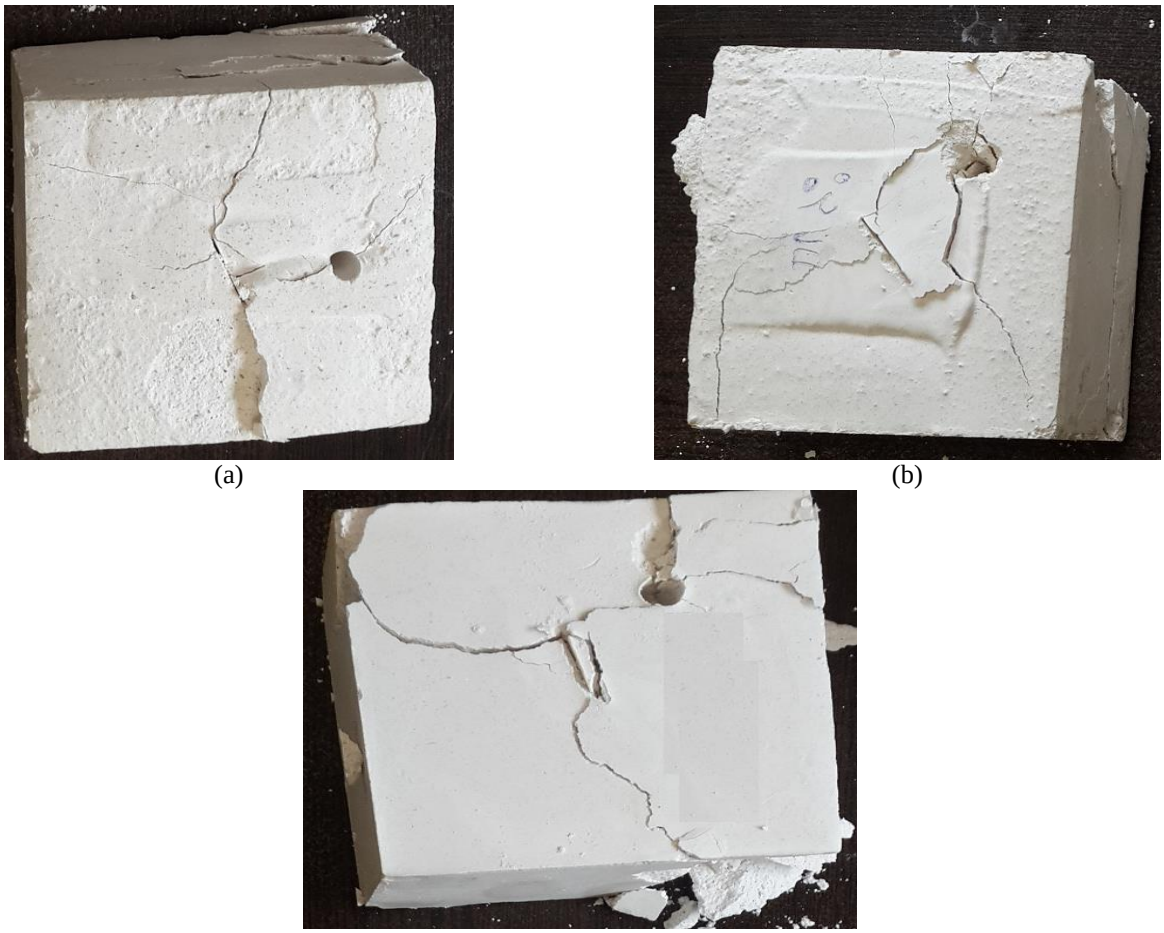

Fig. 6 Failure pattern when Pore was situated (a) 2 cm above the upper notch tip, 2 cm above the middle of the notch and 2 cm above the lower of the notch tip; notch angle is 60°

wing cracks initiate from the hole. One of these crack coalesce with lower tip of the notch and one of them coalescence with sample edge.

When notch angle is 60° and pore was situated 2 cm above the middle of the joint (Fig. 6(b)), two wing crack initiate from the notch and propagate nearly parallel to normal load till coalescence with sample edge. Also two wing cracks initiate from the hole. One of these crack coalescence with lower tip of the notch and one of them coalescence with sample edge.

When notch angle is 60° and pore was situated 2 cm above the lower tip of the joint (Fig. 6(c)), two wing crack initiate from the notch and propagate nearly parallel to normal load till coalescence with sample edge. Also three wing cracks initiate from the hole. One of these crack coalesce with upper tip of the notch and two of them coalescence with sample edge.

4. The bonded particles modeling techniques

The bonded particle algorithm implemented in a particle flow code in two dimensions (PFC2D) which is based on the versatile discontinuous materials (geo materials) known as discrete element method (DEM). Based on this modeling technique, any geo-mechanical problem can be modeled in term of a series of disc particles (circular disc elements for two dimensional problems). These numerically created particles can form different shapes while combining together to constitute particles assembly for modeling the geo-mechanical problem. This procedure allows that each particle assembly behaves like an autonomous object in the numerically modeled specimen. In this numerical modeling each particle assembly can be produced with a uniform size-distribution algorithm to have radii with different dimensions. The particles within the assembly can move individually while they are bonded to each other at the specified contact points. In this discrete element modeling technique each particle assembly generate an individual particle mode for the geo-mechanical problem. As a whole, the bonded particle model can be designed considering the following assumptions: a) each particle act as a rigid body; b) the area of contact points are negligible; c) a soft-contact procedure is adopted; d) overlaps at the contact points are allowed; e) the magnitudes of overlaps are related to the induced forces; f) all overlaps are small compared to the particle's sizes and g) all the particles are bonded at the corresponding contact points.

The contact (normal) and parallel bonds can both be assumed for modeling the particles by the particle bond

modeling technique. The magnitude of the tensile normal force in the case of contact bonds must exceed that of the normal bonding strength of the particles in the assembly. After that the normal and shear contact forces can be set to zero at the breaking stage of the contacts. On the other hand, in case of shear breakage of bonds, the induced shear contact force in between the particle assembly should be equal or exceed that of the shear strength of the particle contacts. In this case, the contact forces are kept constant while the induced shear forces are allowed to exceed that of the frictional and coherent shear strength of the contact particles under compressive normal loading conditions.

In the present study, the micro-mechanical properties of the rock like materials (such as concrete) are predicted by using the parallel bond modeling techniques. Table 2 gives eight micro mechanical parameters of the concrete specimens being used in the present parallel bond model technique. The macro mechanical parameters of the concrete specimens obtained in the laboratory are being calibrated by these numerically evaluated micro parameters. The standard calibration procedure used in this study is the trial and error scheme. The measured experimental results for the macro mechanical parameters of the concrete specimens obtained from the laboratory tests are already known and can be used in this iteration process. In this procedure, the elastic modulus of the intact material is related to that of the bonded particle model. In addition, the shear and normal strengths of the particle bonding are also related to those of bonded particle model, in this research.

4.1 Preparing the modeled samples and calibrating the numerical modeling

The standard process of generating a suitable particle assembly model in the particle flow code, was explained by Itasca (1999). The same procedure is adopted in the present study by assuming the following steps: i) generating and packing of the particles with in the assembly, ii) stress initialization by assuming isotropic loading conditions, iii) eliminating the floating particles with in the assembly, iv) installing the bonds with in the particles of the assembly and v) the effects of gravity are neglected because the gravity induced stress gradient is very small and have a relatively negligible effect on the macroscopic behavior of the concrete specimens.

Table 2 Micro properties used to represent the concrete specimens modeled having a tensile strength of 1.6 MPa

property	value	property	value
Type of particle	disc	Parallel bond radius muliplier	1.4
Densiy (kg/m3)	2000	Youngs modulus of parallel bond (GPa)	40
Minimum radius (mm)	0.27	Parallel bond stifness ratio (pb_kn/pb_ks)	1.7
Size ratio	1.56	Particle friction coefficien	0.4
Porosity ratio	0.08	Parallel normal strength, mean (MPa)	8
Local damping coefficient	0.7	Parallel normal strength, std. dev (MPa)	2
Contact young modulus (GPa)	4	Parallel shear strength, mean (MPa)	8
Stiffness ratio (kn/ks)	1.7	Parallel shear strength, std. dev (MPa)	2

In the present study, the unconfined compressive strength test, the indirect tensile strength (Brazilian) test and the biaxial stress test were carried out in a rock mechanics laboratory. The measured macroscopic mechanical properties were used to calibrate the microscopic properties of the particles considering the parallel bond model of bonded particle model technic. A relatively small loading rate (0.016 m/s) was applied in all models simulated in this study as suggested by Potyondy (2004) and Ghazvinian (2012). The micro and macro mechanical properties of the modeled concrete samples were calibrated by the standard trial and error calibration process. Table 3 represents the micro properties used for the simulation of the concrete samples with 1.6 MPa in tensile strength.

Following sections summarize the specifications of different numerical tests adopted for the calibration of the models used in this research.

The lines

4.1.1 Numerical modeling of unconfined compressive strength test

The conventional unconfined compressive strength test can be simplified to model by a particle flow code (PFC2D). The particle assembly as illustrated in Fig. 7(a) is modelled such that two moving walls compress the assembly. The lines in this figure indicate the bonds and the positions of micro cracks existing in the particle assembly. The black and red lines represent the tensile and shear failure of the modeled specimen, respectively. The walls acting as frictionless rigid plates enclosing the modeled concrete specimen. The height of the particle assembly representing the tested concrete specimen is 108 mm and the specimen's width is 54 mm. The assembly consists of 14298 particles with a normal particle size distribution ranging in radii from 0.27 to 0.421 mm. The radii of particle bonds were chosen to be as small as possible so that they may not affect the computational efficiency and minimize the total running time of the computer code. Assuming a dense packing of the modeled concrete specimen, a reasonable porosity ratio of 0.08 is considered in this work. The Poisson's ratio, the elastic modulus, E, the unconfined compressive strength (UCS) and the crack initiation stress for the particle assembly can be easily estimated through the numerical simulation of the modeled sample by PFC2D (Potyondy 2004). However, as shown in Fig. 7(b), the failure plane estimated by the numerical modeling is nearly vertical which is in agreement with the experimentally observed one in the laboratory.

Table 3 gives the numerical results and compares them with those measured experimentally through laboratory tests.

Table 3 Macro mechanical properties of model material in Experimental test and PFC2D

Mechanical properties	Experimental results	PFC2D model results
Elastic modulus (GPa)	17	17
Poissons ratio	0.18	0.19
UCS (MPa)	10	10
Crack initiation stress (MPa)	7	7
Brazilian tensile strength (MPa)	1.3	1.2
Friction angle	29	28
Cohesion (MPa)	3	3

4.1.2 Numerical simulation of Brazilian tensile strength test

The standard indirect tensile strength test known as Brazilian test was used in this study to calibrate the tensile strength of the concrete specimens modeled by the two dimensional particle flow code. The specimen's diameter for Brazilian tensile strength (BTS) test was 54 mm and 5615 particles were used to simulate this test. This particle assembly was crushed by moving the lateral walls toward each other with a standard speed of 0.016 m/s. The failure patterns for both numerical and experimental concrete specimens are shown in Figs. 7(c) and 7(d), respectively. Horizontal splitting planes resulted in this modeling research are in good agreement with those observed experimentally through laboratory tests. Fig. 7(e) shows the numerical BTS results which are compared with those obtained experimentally.

4.1.3 Numerical simulation of biaxial test for concrete specimens

The experimental requirements for performing the biaxial tests in the laboratory are initially the same as those for uniaxial compressive tests. For a two dimensional modeling of this test, a rectangular model was prepared and loaded from four sides by the surrounding walls. In this case the top and bottom walls serve as the vertical loading platens but the two modeled specimens sides serve as the applied confining stress walls. For simulating a soft confinement, the normal stiffness for the lateral walls was set as 0.001 to 0.2 times the average normal stiffness of the specimen. The servo-mechanism (which controls the velocities of the four confining walls of the modeled concrete specimen) was activated to apply the suitable vertical and confined stresses to the modeled particle assembly. Effects of confined stress on the strength parameters of the modeled specimens are shown in Fig. 7(f). The behavior of the modeled specimens under biaxial loading condition then can be obtained from PFC2D and these results can be compared with those measured experimentally through real tests already presented in Table 3. Comparing the numerical and experimental results (already given in Table 3) demonstrate that the results obtained through the numerical modelling approach are very close to those measured experimentally.

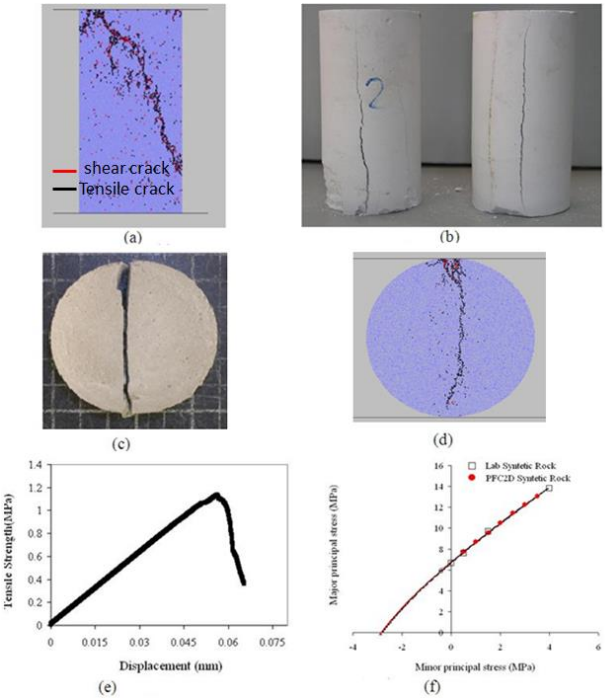

Fig. 7 (a) Unconfined compressive test (cracks described by red/black lines), (b) failure pattern in physical uniaxial sample, (c) failure pattern in PFC2D model, (d) failure pattern in physical sample, (e) Tensile strength versus axial displacement curve for numerical Brazilian test simulation) Calibrated failure locus for PFC synthetic rock compared to the Laboratory measured

This procedure helps to the verification and calibration of the proposed numerical method applied in this research.

4.2 Simulating the uniaxial compressive strength test for specimens with crack-pore

After calibration of PFC2D, the calibrated micro parameters were used in PFC2D models (Figs. 8-10). The PFC specimen has the cross sectional dimensions (54×108 mm). To create the models, a total of 11179 disks with a minimum radius of 0.27 mm were used. The cracks and pores are formed in the model, by deleting bands of the particles, with a width of 1 mm, from the model. Totally, nine rectangular models were constructed. Each model contains crack and pore. The size of the cracks was 2cm and its orientation was 30 (Fig. 8), 45 (Fig. 9) and 60 (Fig. 10). Diameter of pore was 1 cm which situated at the upper of the notch i.e., 2 cm above the upper notch tip, 2 cm above the middle of the notch and 2 cm above the lower of the notch tip. The uniaxial test was simulated by making the platens approaching each other with the rate of 0.016 m/s. The axial displacement was measured by monitoring the upper and lower wall displacements.

(a) (b) (c)

Fig. 8 Pore was situated (a) 2 cm above the upper notch tip, 2 cm above the middle of the notch and 2 cm above the lower of the notch tip; notch angle is 30°

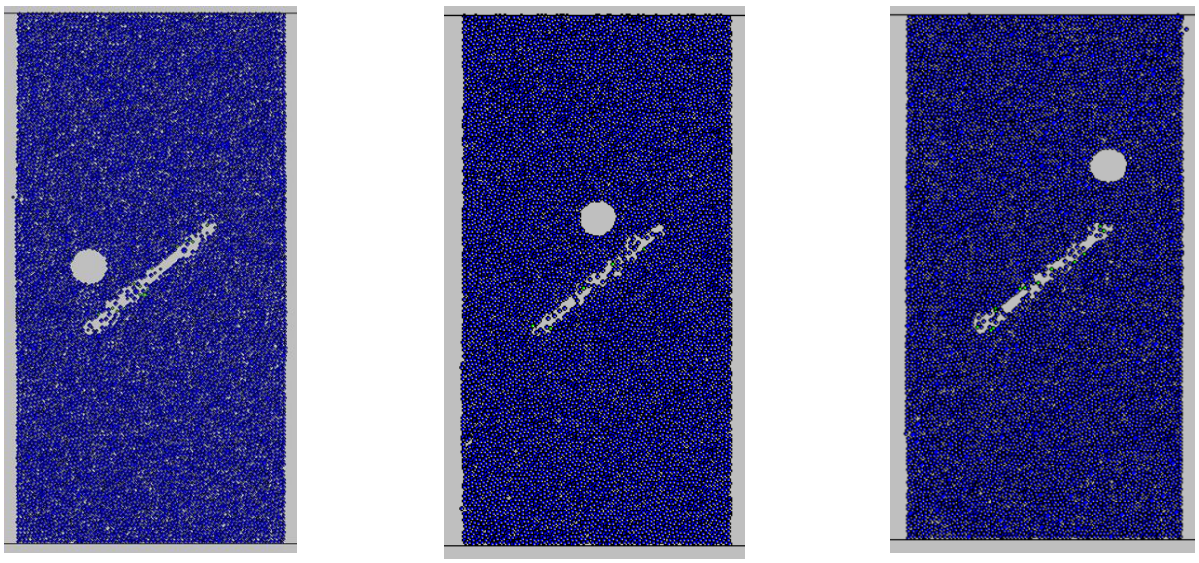

(a) (b) (c)

Fig. 9 Pore was situated (a) 2 cm above the upper notch tip, 2 cm above the middle of the notch and 2 cm above the lower of the notch tip; notch angle is 45°

5. Results and discussion

5.1 Failure patterns in the numerical models of cracked-pored specimens

Figs. 11-13 show the interaction between pore and notch for three different value of notch angle, i.e., 30, 45 and 60, respectively. Tensile and shear cracks are shown by black and red lines, respectively.

5.1.1 Specimens containing a 30° notch

When notch angle is 30° and pore was situated 2 cm above the lower tip of the joint (Fig. 11(a)), One wing crack initiates from upper tip of the notch and propagates diagonally till coalescence with model edge. Also two wing crack initiates from lower tip of the notch and propagates diagonally till coalescence with model edge. One wing crack initiates from lower wall of the notch. Two wing cracks initiates from upper and lower of the pore. These cracks propagate parallel to loading axis. Lower tensile crack coalesces with the lower tip of the notch.

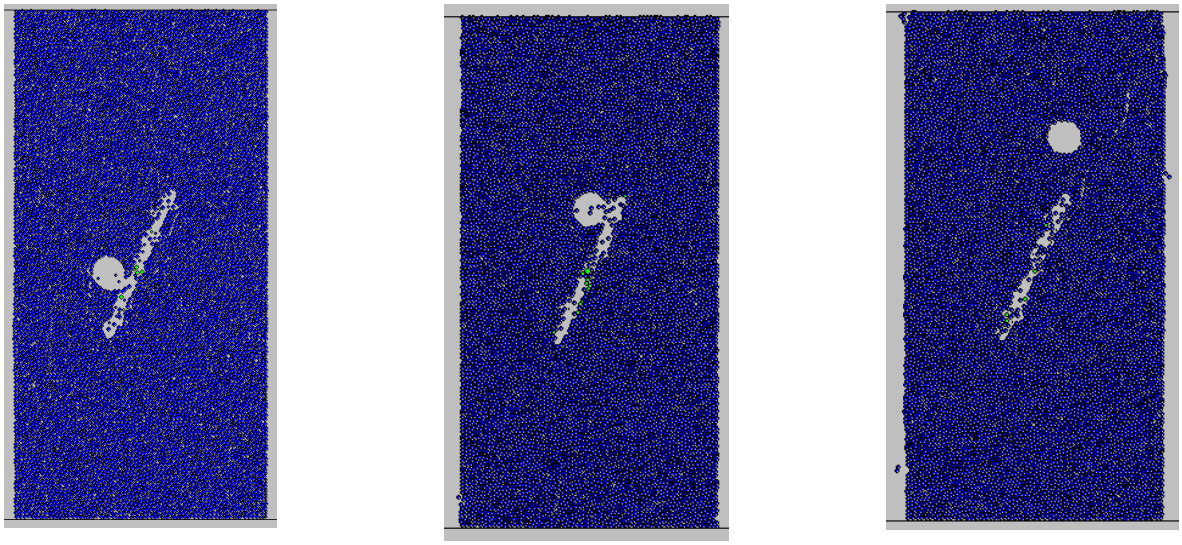

(a) (b) (c)

Fig. 10 Pore was situated (a) 2 cm above the upper notch tip, 2 cm above the middle of the notch and 2 cm above the lower of the notch tip; notch angle is 60°

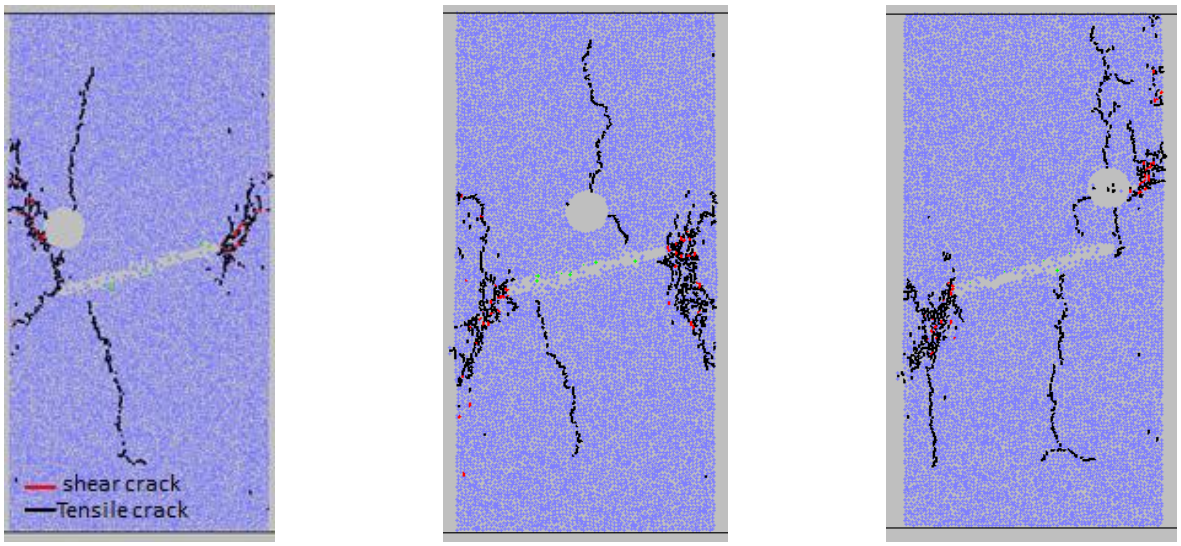

(a) (b) (c)

Fig. 11 Failure pattern when pore was situated (a) 2 cm above the upper notch tip, 2 cm above the middle of the notch and 2 cm above the lower of the notch tip; notch angle is 30°

When notch angle is 30° and pore was situated 2 cm above the middle of the joint (Fig. 11(b)), two wing crack initiates from upper tip of the notch and two wing cracks initiate from lower tip of the notch. These cracks propagate diagonally till coalescence with model edge. One wing crack initiates from lower wall of the notch. Two wing cracks initiates from upper and lower of the pore. These cracks propagate parallel to loading axis. Lower tensile wing crack coalesce with the upper wall of the notch.

When notch angle is 30° and pore was situated 2 cm above the upper tip of the joint (Fig. 11(c)), two wing crack initiates from lower tip of the notch and propagate diagonally till coalescence with model edge. One wing crack initiates from lower wall of the notch and propagates parallel o loading axis. Also four wing cracks initiates from upper, lower, left and right side of the pore. These cracks propagate parallel to loading axis. Two of these tensile wing crack coalescences with the upper wall of the notch. One of them propagates vertically upward and other crack propagates diagonally till coalescence with model edge.

5.1.2 Specimens containing a 45° notch

When notch angle is 45° and pore was situated 2 cm above the lower tip of the joint (Fig. 12(a)), four wing crack initiates at tip of the notch. One of these wing cracks propagates diagonally ill coalescence with model edge. Also

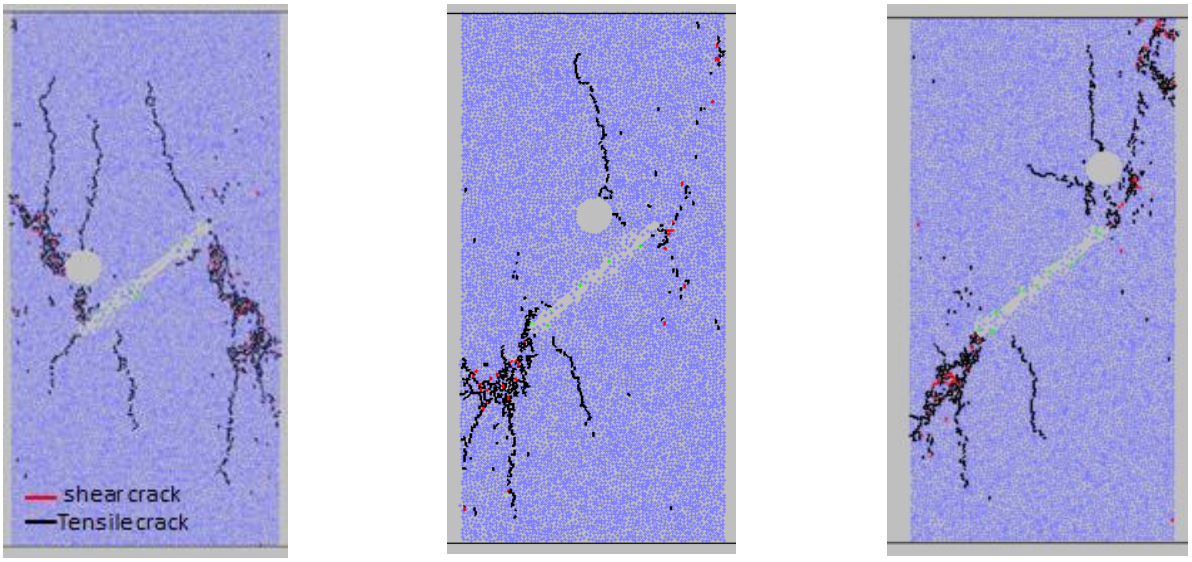

(a) (b) (c)

Fig. 12 Failure pattern when Pore was situated (a) 2 cm above the upper notch tip, 2 cm above the middle of the notch and 2 cm above the lower of the notch tip; notch angle is 45°

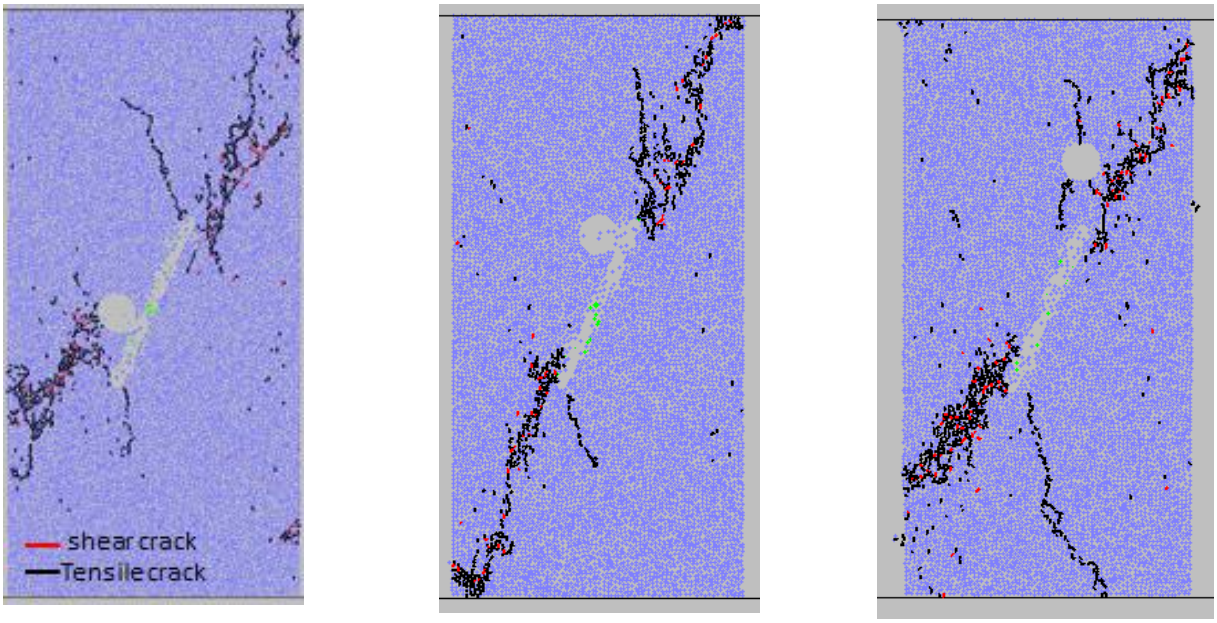

(a) (b) (c)

Fig. 13 Failure pattern when Pore was situated (a) 2 cm above the upper notch tip, 2 cm above the middle of the notch and 2 cm above the lower of the notch tip; notch angle is 60°

here wing crack initiates from hole. The lower wing crack propagates vertically related to loading axis till coalescence with notch.

When notch angle is 45° and pore was situated 2 cm above the middle of the joint (Fig. 12(b)), wing crack initiates from lower tip of the notch. These cracks propagate diagonally till coalescence with the model edge. Also two wing crack initiates from hole and propagate parallel to loading axis. Lower wing crack was coalescence with the notch. When notch angle is 45° and pore was situated 2 cm above the upper tip of the joint (Fig. 12(c)), three wing crack initiates from lower tip and upper tip of the notch. These cracks propagate diagonally till coalescence with the model edge. Also three wing crack initiates from the hole and propagate parallel to loading axis. Lower wing crack was coalescence with the notch.

5.1.3 Specimens containing a 60° notch

When notch angle is 60° and pore was situated 2 cm above the lower tip of the joint (Fig. 13(a)), three wing

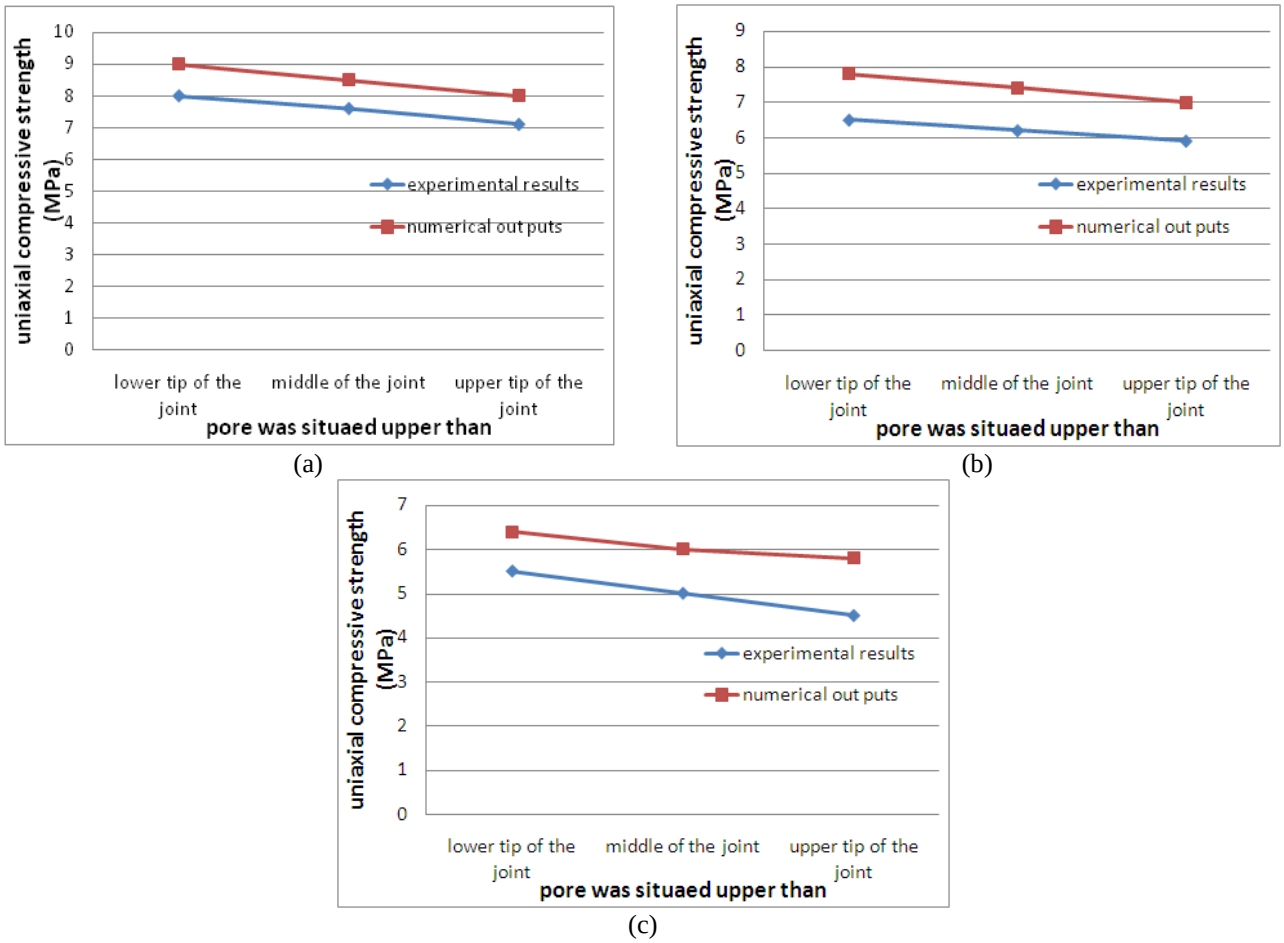

Fig. 14 The effect of pore-crack interaction on the uniaxial compressive strength for three different joint angularities of (a) 30°, (b) 45° and (c) 60°.

crack initiates from lower tip and upper tip of the notch. One of these cracks propagates diagonally till coalescence with the model edge. Also one wing crack initiates from the left side of the hole and propagate diagonally till coalescence with the model edge.

When notch angle is 60° and pore was situated 2 cm above the middle of the joint (Fig. 13(b)), two wing crack initiates from lower tip and upper tip of the notch. These cracks propagate diagonally till coalescence with the model edge.

When notch angle is 60° and pore was situated 2 cm above the upper tip of the joint (Fig. 13(c)), three wing crack initiates from lower tip and upper tip of the notch. One of these cracks propagates vertically related to normal loading till coalescence with model edge. Two other wing cracks propagate diagonally till coalescence with the model edge. Also four wing crack initiates from the hole. Two of these wing cracks coalescence with upper oriented wing cracks. One of them coalescence with upper wall of the notch and finally the forth wing crack propagates vertically through the model.

With comparison between numerical results (Figs. 11-13) and experimental measurements (Figs. 4-6) its clear that the good accordance was established between them.

5.2 Effects of pore-crack interaction on the uniaxial compressive strength of modelled concrete specimens

Figs. 14(a)-14(c) show the effect of pore-crack interaction on the uniaxial compressive strength for three different joint angularities of 30°, 45° and 60°, respectively. Each figure shows experimental and numerical results for three pore configuration, i.e. when pore was situated 2 cm below, at the middle and above the joint.

From Fig. 14, it's clear that the uniaxial compressive strength has maximum value when pore was situated upper than lower tip of the joint. The uniaxial compressive strength was decreased By changing the pore situation from lower tip of the joint to upper tip of the joint. Also uniaxial strength was decreased by increasing the joint angularities from 30° to 60°. With comparison between numerical results and experimental measurements it's clear that the good accordance was established between them.

5. Conclusions

- Generally, two wing cracks initiate from notch tips and propagate nearly parallel to normal load till coalescence with sample edge. Also two wing cracks

initiate from the hole. One of these crack coalescence with the notch and one of them coalescence with sample edge. Number of wing cracks was increased by increasing the joint angle. Also number of wing cracks was increased by changing the pore situation from lower tip of the joint to upper tip of the joint.

- With comparison between numerical failure pattern and experimental measurements its clear that the good accordance was established between them.
- The uniaxial compressive strength has maximum value when pore was situated upper than lower tip of the joint.
- The uniaxial compressive strength was decreased By changing the pore situation from lower tip of the joint to upper tip of the joint.
- uniaxial strength was decreased by increasing the joint angularities from 30° to 60°.
- With comparison between numerical results and experimental measurements its clear that the good accordance was established between them.

References

Abdollahipour, A., Marji, M.F., Bafghi, A.Y. and Gholamnejad, J. (2015), "Simulating the propagation of hydraulic fractures from a circular wellbore using the Displacement Discontinuity Method", *Int. J. Rock Mech. Min. Sci*., **80**, 281-291. https://doi.org/10.1016/j.ijrmms.2015.10.004.

Antunes, F.V. and Rodrigues, D.M. (2008), "Numerical simulation of plasticity induced crack closure: Identification and discussion of parameters", *Eng. Fract. Mech*., **75**(10), 3101-3120. https://doi.org/10.1016/j.engfracmech.2007.12.009.

ASTM E1681 (2008), "Standard test method for determining threshold stress intensity factor for environment-assisted cracking of metallic materials", The American Society for Testing and Materials.

Backers, T., Dresen, G., Rybacki, E. and Stephansson, O. (2004), "New data on mode II fracture toughness of rock from the punchthrough shear test", *Int. J. Rock Mech. Min. Sci*., **41**(1), 2-7.

Barry, N.W., Raghu, N.S. and Gexin, S. (1992), Rock Fracture Mechanics Principles Design and Applications, Amsterdam, Elsevier.

Becker, A.A. (1992), The Boundary Element Method in Engineering: a Complete Course, McGraw-Hill Companies.

Bi, J.; Zhou, X.P. and Xu, X.M. (2017), "Numerical simulation of failure process of rock-like materials subjected to impact loads", *Int. J. Geomech*., **17**(3), 04016073. https://doi.org/10.1061/(ASCE)GM.1943-5622.0000769.

Bi, J.; Zhou, X.P. and Qian, Q.H. (2016), "The 3D numerical simulation for the propagation process of multiple pre-existing flaws in rock-like materials subjected to biaxial compressive loads", *Rock Mech. Rock Eng*., **49**(5), 1611-1627.

Bian, L.C. and Kim, K.S. (2004),"The minimum plastic zone radius criterion for crack initiation direction applied to surface cracks and through-cracks under mixed mode loading", *Int. J. Fatigue*, **26**(11), 1169-1178. https://doi.org/10.1016/j.ijfatigue.2004.04.006.

Botvina, L.R. and Korsunsky, A.M. (2005), "On the structure of plastic and damage zones in different materials and at various scales", *Proceedings of the 6th International Conference on Fracture*.

Boumaaza, M., Bezazi, A., Bouchelaghem, H., Benzennache, N., Amziane, S. and Scarpa, F. (2017), "Behavior of pre-cracked deep beams with composite materials repairs", *Struct. Eng. Mech.*, **63**(5), 43-56. https://doi.org/10.12989/sem.2017.63.5.575.

Caputo, F., Lamanna, G. and Soprano, A. (2012), "Geometrical parameters influencing a hybrid mechanical coupling", *Key Eng. Mater*., 525-526.

Caputo, F., Lamanna, G. and Soprano, A. (2013), "On the evaluation of the plastic zone size at the crack tip", *Eng. Fract. Mech*., **103**, 162-173. https://doi.org/10.1016/j.engfracmech.2012.09.030.

Cheng, H., Zhou, X.P., Zhu, J. and Qian, Q. (2016), "The effects of crack openings on crack initiation, propagation and coalescence behavior in rock-like materials under uniaxial compression", *Rock Mech. Rock Eng*., **49**(9), 3481-3494.

Cheng, H. and Zhou, X.P. (2015), "A multi-dimensional space method for dynamic cracks problems using implicit time scheme in the framework of the extended finite element method", *Int. J. Damage Mech*., **24**(6), 859-890. https://doi.org/10.1177/1056789514555149.

de Castro, J.T.P., Meggiolaro, M.A. and de Oliveira Miranda, A.C. (2009), "Fatigue crack growth predictions based on damage accumulation calculations ahead of the crack tip", *Compos. Mater. Sc*i., **46**(1), 115-123. https://doi.org/10.1016/j.commatsci.2009.02.012.

Fowell, R.J. (1995), "Suggested method for determining mode I fracture toughness using cracked chevron notched Brazilian disc (CCNBD) specimens", *Int. J. Rock Mech. Min. Sci. Geomech. Abst*., **32**(1), 57-64

Haeri, H., Shahriar, K., Marji, M.F. and Moarefvand, P. (2014), "Investigation of fracturing process of rock-like Brazilian disks containing three parallel cracks under compressive line loading", *Strength of Mater*., **46** (3), 404-416..

Haeri, H., Marji, M.F. and Shahriar, K. (2015a), "Simulating the effect of disc erosion in TBM disc cutters by a semi-infinite DDM", *Arabian J. Geosci*., **8**(6), 3915-3927.

Haeri, H., Khaloo, A. and Marji, M.F. (2015b), "Experimental and numerical analysis of Brazilian discs with multiple parallel cracks", *Arabian J. Geosci*., **8**(8), 5897-5908.

Haeri, H., Sarfarazi, V. and Hedayat, A. (2016a), "Suggesting a new testing device for determination of tensile strength of concrete", *Struct. Eng. Mech*., **60**(6), 939-952. https://doi.org/10.12989/sem.2016.60.6.939.

Haeri, H., Sarfarazi, V., Marji, M.F., Hedayat, A. and Zhu, Z. (2016b), "Experimental and numerical study of shear fracture in brittle materials with interference of initial double cracks", *Acta Mech. Solida*, **29**(5), 555-566. https://doi.org/10.1016/S0894-9166(16)30273-7.

Hori, M. and Nemat-Nasser, S. (1987), "Interacting micro-cracks near the tip in the process zone of a macro-crack", *J. Mech. Phys. Solid*., **35**(5), 601-629. https://doi.org/10.1016/0022-5096(87)90019-6.

Huang, Y., Chen, J. and Liu, G. (2010), "A new method of plastic zone size determined based on maximum crack opening displacement", *Eng. Fract. Mech*., **77**(14), 2912-2918. https://doi.org/10.1016/j.engfracmech.2010.06.026.

Jiang, Z., Wan, S., Zhong, Z., Li, M. and Shen, K. (2014), "Determination of mode-I fracture toughness and non-uniformity for GFRP double cantilever beam specimens with an adhesive layer", *Eng. Fract. Mech.*, **128**, 139-156. https://doi.org/10.1016/j.engfracmech.2014.07.011

Khodayar, A. and Nejati, H.R. (2018), "Effect of thermal-induced microcracks on the failure mechanism of rock specimens", *Comput. Concrete*, **22**(1), 93-100. https://doi.org/10.12989/cac.2018.22.1.093.

Kuang, J.H. and Chen, Y.C. (1997), "The tip pf plastic energy applied to ductile fracture initiation under mixed mode loading", *Eng. Fract. Mech*., **58**(1-2), 61-70.

https://doi.org/10.1016/S0013-7944(97)00073-8.
Kudari, S.K., Maiti, B. and Ray, K.K. (2010), "Experimental investigation on possible dependence of plastic zone size on specimen geometry", Frattura ed Integrità Strutturale: Annals, 3.
Mechanics, F. (1995), Fundamentals and Applications, TL Anderson.
Nabil, B., Abdelkader, B., Miloud, A. and Noureddine, B. (2012), "On the mixed-mode crack propagation in FGMs plates: comparison of different criteria", *Struct. Eng. Mech.*, **61**(3), 201-213. https://doi.org/10.12989/sem.2017.61.3.371.
Newman, J.C., Dawicke, D.S. and Bigelow, C.A. (1992), "Finite-element analyses and fracture simulation in thin-sheet aluminum alloy", National Aeronautics and Space Administration, Langley Research Center.
Noël, M. and Soudki, K. (2014), "Estimation of the crack width and deformation of FRP-reinforced concrete flexural members with and without transverse shear reinforcement", *Eng. Struct.*, **59**, 393-398. https://doi.org/10.1016/j.engstruct.2013.11.005.
Marji, M.F. (2014), "Numerical analysis of quasi-static crack branching in brittle solids by a modified displacement discontinuity method", *Int. J. Solids Struct.*, **51**(9), 1716-1736. https://doi.org/10.1016/j.ijsolstr.2014.01.022.
Monfared, M.M. (2017), "Mode III SIFs for interface cracks in an FGM coating-substrate system", *Struct. Eng. Mech.*, **64**(1), 78-95. https://doi.org/10.12989/sem.2017.64.1.071.
Nejati, H.R. and Ghazvinian, A. (2014), "Brittleness effect on rock fatigue damage evolution", *Rock Mech. Rock Eng.*, **47**(5), 1839–1848
Ouchterlony, F. (1988), "Suggested methods for determining the fracture toughness of rock", *Int. J Rock Mech. Min. Sci.*, **25**(2), 71-96.
Oudad, W., Bouiadjra, B.B., Belhouari, M., Touzain, S. and Feaugas, X. (2009), "Analysis of the plastic zone size ahead of repaired cracks with bonded composite patch of metallic aircraft structures", *Comput. Mater. Sci.*, **46**(4), 950-954. https://doi.org/10.1016/j.commatsci.2009.04.041.
Panaghi, K., Golshani, A. and Takemura , T. (2015), "Rock failure assessment based on crack density and anisotropy index variations during triaxial loading tests", *Geomech. Eng.*, **9**, 793-813. https://doi.org/10.12989/gae.2015.9.6.793.
Pan, B., Gao, Y. and Zhong, Y. (2014), "Theoretical analysis of overlay resisting crack propagation in old cement concrete pavement", *Struct. Eng. Mech.*, **52**(4), 167-181. DOI: http://dx.doi.org/10.12989/sem.2014.52.4.829.
Rans, C.D. and Alderliesten, R.C. (2009), "Formulating an effective strain energy release rate for a linear elastic fracture mechanics description of delamination growth", *Proceedings of the 17th International Conference on Composite Materials (ICCM-17)*.
Rao, Q. (1999), "Pure shear fracture of brittle rock", Doctoral Dissertation, Division of Rock Mechanics, Luleå University, Sweden.
Rao, Q., Sun, Z., Stephansson, O., Li, C. and Stillborg, B. (2003), "Shear fracture (Mode II) of brittle rock", *Int. J. Rock Mech. Min. Sci.*, **40**(3), 355-375. https://doi.org/10.1016/S1365-1609(03)00003-0.
Ramadoss, P. and Nagamani, K. (2013), "Stress-strain behavior and toughness of high-performance steel fiber reinforced concrete in compression", *Comput. Concrete*, **11**(2), 55-65. https://doi.org/10.12989/cac.2013.11.2.149.
Rice, J. and Rosengren, G.F. (1968), "Plane strain deformation near a crack tip in a power-law hardening material", *J. Mech. Phys. Solids.*, **16**(1), 1-12. https://doi.org/10.1016/0022-5096(68)90013-6.
Rose, L.R.F. (1986), "Microcrack interaction with a main crack", *Int. J. Fract.*, **31**(3), 233-242.
Rooh, A., Nejati, H. and Goshtasbi, K. (2018), "A new formulation for calculation of longitudinal displacement profile (LDP) on the basis of rock mass quality", *Geomech. Eng.*, **16**(5), 539-545. DOI: https://doi.org/10.12989/gae.2018.16.5.539.
Rubinstein, A.A. (1986), "Macrocrack-microdefect interaction", *J. Appl. Mech.*, **53**(3), 505-510. doi:10.1115/1.3171803.
Sarfarazi, V. and Haeri, H.A. (2016), "Review of experimental and numerical investigations about crack propagation", *Comput. Concrete*, **18**(2), 235-266. http://dx.doi.org/10.12989/cac.2016.18.2.235
Sousa, R.A., Castro, J.T.P., Lopes, A.A.O. and Martha, L.F. (2013), "On improved crack tip plastic zone estimates based on T-stress and on complete stress fields", *Fatigue Fract. Eng. M.*, **36**(1), 25-38. https://doi.org/10.1111/j.1460-2695.2012.01684.x.
Tong, Y.C., Hu, W. and Mongru, D. (2007), A Crack Growth Rate Conversion Module: Theory, Development, User Guide and Examples, Air Vehicles Division, Defence Science and Technology Organisation, Victoria, Australia.
Wang, R. and Kemeny, J.M. (1994), "A study of the coupling between mechanical loading and flow properties in tuffaceous rock", *Proceedings of the 1st North American Rock Mechanics Symposium*, American Rock Mechanics Association.
Wang, Y., Zhou, X.P. and Xu, X. (2016), "Numerical simulation of propagation and coalescence of flaws in rock materials under compressive loads using the extended non-ordinary state-based peridynamics", *Eng. Fract. Mech.*, **163**, 248-273. https://doi.org/10.1016/j.engfracmech.2016.06.013.
Wang, Y., Zhou, X.P. and Shou, Y. (2017), "The modeling of crack propagation and coalescence in rocks under uniaxial compression using the novel conjugated bond-based peridynamics", *Int. J. Mech. Sci.*, **128**, 614-643.
Wang, Y., Zhou, X.P., Wang, Y. and Shou, Y. (2018), "A 3-D conjugated bond-pair-based peridynamic formulation for initiation and propagation of cracks in brittle solids", *Int. J. Solids Struct.*, **134**, 89-115. https://doi.org/10.1016/j.ijsolstr.2017.10.022.
Wang, Y., Zhou, X.P. and Kou, M. (2018), "Peridynamic investigation on thermal fracturing behavior of ceramic nuclear fuel pellets under power cycles", *Ceramics Int.*, **44**(10), 11512-11542. https://doi.org/10.1016/j.ceramint.2018.03.214.
Xin, G., Hangong, W., Xingwu, K. and Liangzhou, J. (2010), "Analytic solutions to crack tip plastic zone under various loading conditions", *Eur. J. Mech. A-Solid.*, **29**(4), 738-745. https://doi.org/10.1016/j.euromechsol.2010.03.003.
Yang, S.Q. (2011), "Crack coalescence behavior of brittle sandstone samples containing two coplanar fissures in the process of deformation failure", *Eng. Fract. Mech.*, **78**(17), 3059-3081. https://doi.org/10.1016/j.engfracmech.2011.09.002.
Yoshihara, H. (2013), "Initiation and propagation fracture toughness of solid wood under the mixed Mode I/II condition examined by mixed-mode bending test", *Eng. Fract. Mech.*, **104**, 1-15. https://doi.org/10.1016/j.engfracmech.2013.03.023.
Zeng, G., Yang, X., Yin, A. and Bai, F. (2014), "Simulation of damage evolution and crack propagation in three-point bending pre-cracked asphalt mixture beam", *Constr. Build. Mater.*, **55**, 323-332. https://doi.org/10.1016/j.conbuildmat.2014.01.058.
Zhao, X.L., Roegiers, J.C. and Guo, M. (1990), "The determination of fracture toughness of rocks chevron-notched Brazilian disk specimens", *Proceedings of the 4th Annual SCA Technical Conference*, Dallas, Texas, USA.
Zhou, X.P., Zhang, J. and Wong, L. (2018a), "Experimental study on the growth, coalescence and wrapping behaviors of 3D cross-embedded flaws under uniaxial compression", *Rock Mech. Rock Eng.*, **51**(5), 1379-1400
Zhang, J., Zhou, X.P., Zhu, J., Xian, C. and Wang, Y. (2018), "Quasi-static fracturing in double-flawed specimens under uniaxial loading: the role of strain rate", *Int. J. Fracture*, **211**(1-2), 75-102.

Zhou, X., Zhang, J., Yang, L. and Cui, Y. (2018b), "Internal morphology of cracking of two 3-D pre-existing cross-embedded flaws under uniaxial compression", *Geotech. Test. J.*, **41**(2), 329-339. DOI: 10.1520/GTJ20170189.

CC